Impact of CYGNSS-Derived Winds on Tropical Cyclone Forecasts in a Global and Regional Model

MICHAEL J. MUELLER,[a,b] BACHIR ANNANE,[b,c] S. MARK LEIDNER,[d] AND LIDIA CUCURULL[b]

[a] *University Corporation for Atmospheric Research, Boulder, Colorado*
[b] *NOAA/OAR/Atlantic Oceanographic and Meteorological Laboratory, Miami, Florida*
[c] *Cooperative Institute for Marine and Atmospheric Studies, University of Miami, Miami, Florida*
[d] *Atmospheric and Environmental Research, Lexington, Massachusetts*

(Manuscript received 22 April 2021, in final form 1 August 2021)

ABSTRACT: An observing system experiment was conducted to assess the impact of wind products derived from the Cyclone Global Navigation Satellite System (CYGNSS) on tropical cyclone track, maximum 10-m wind speed V_{max}, and minimum sea level pressure forecasts. The experiment used a global data assimilation and forecast system, and the impact of both CYGNSS-derived scalar and vector wind retrievals was investigated. The CYGNSS-derived vector wind products were generated by optimally combining the scalar winds and a gridded a priori vector field. Additional tests investigated the impact of CYGNSS data on a regional model through the impact of lateral boundary and initial conditions from the global model during the developmental phase of Hurricane Michael (2018). In the global model, statistically significant track forecast improvements of 20–40 km were found in the first 60 h. The V_{max} forecasts showed some significant degradations of ~2 kt at a few lead times, especially in the first 24 h. At most lead times, impacts were not statistically significant. Degradations in V_{max} for Hurricane Michael in the global model were largely attributable to a failure of the CYGNSS-derived scalar wind test to produce rapid intensification in the forecast initialized at 0000 UTC 7 October. The storm in this test was notably less organized and symmetrical than in the control and CYGNSS-derived vector wind test. The regional model used initial and lateral boundary conditions from the global control and CYGNSS scalar wind tests. The regional forecasts showed large improvements in track, V_{max}, and minimum sea level pressure.

KEYWORDS: Atmosphere; Tropical cyclones; Satellite observations; Data assimilation; Numerical weather prediction/forecasting

1. Introduction

Tropical cyclones (TCs) are one of the most economically destructive and deadly weather events (WHO 2020; WMO 2020). As a result, intensive research has been undertaken to improve tropical cyclone forecasts (e.g., Leroux et al. 2018 and references therein). Unfortunately, TC track and especially intensity (e.g., maximum 10-m wind speed V_{max}) have proven difficult to forecast. While track forecasts have improved in the past several decades, improvements in V_{max} have been more difficult to achieve. This difficulty is due in part to the fact that TCs frequently develop in the often observation-sparse tropical oceans. Hence, a major task for atmospheric science is to fill in the gaps of the global observing system, especially in the vicinity of developing TCs over the tropical oceans.

Given the remoteness of these regions, frequent in situ observations are not feasible. Observational data from reconnaissance missions can be obtained in some cases, but are not continuously available. Instead, the key to better observations of all phases of TC development is satellite-based remote sensing. The global satellite-based observing system is currently primarily composed of instruments on geostationary and polar-orbiting satellites that measure visible, infrared, and microwave radiation. These observations are used in a variety of ways to improve diagnosis and prognosis of TCs. For instance, the intensity of a TC has to frequently be estimated in the absence of in situ measurements using visible and infrared satellite imagery to detect patterns in the central dense overcast and eye structure (Dvorak 1984; Velden et al. 2006). This method has been continually evolving since first pioneered in the 1970s and is still used extensively at TC forecast centers such as the National Hurricane Center (NHC) and the Joint Typhoon Warning Center (JTWC). In addition, prognosis of global weather patterns has been improved over the last several decades by ingesting satellite-based radiances into global and regional data assimilation systems at numerical modeling centers around the world (Kalnay 2002). This is especially beneficial where in situ observations have traditionally been sparse (e.g., the Southern Hemisphere and over the open ocean).

Other satellite-based sensors measure the refraction of radio signals emitted by Global Navigation Satellite System (GNSS) satellites as they pass through the atmosphere, a technique known as radio occultation. This occurs when a receiving satellite rises or sets below Earth's limb with respect to the GNSS transmitter. One benefit of exploiting radio occultation for TC forecasts is that radio waves at GNSS frequencies are minimally affected by clouds and precipitation, making it a promising technique for further improvement of TC forecasts. Research on the impact of radio occultation observations on TC forecasts has so far yielded mixed results and has generally focused on the impact of limited radio occultation datasets for individual TC cases (e.g., Huang et al. 2005; Kuo et al. 2009;

Corresponding author: Michael J. Mueller, michael.mueller@noaa.gov

DOI: 10.1175/MWR-D-21-0094.1

Huang et al. 2010; Liu et al. 2012; Anisetty et al. 2014; Chen et al. 2015; Phunthirawuthi et al. 2016).

GNSS signals can also be used to measure the reflection of the signals off Earth's water surfaces. Through the principles of reflectometry, the strength of forward-scattered GNSS signals can be related to the surface roughness of water and therefore near-surface wind speed. Generally, a weaker received signal is indicative of a rougher water surface and stronger near-surface winds (i.e., more scattering of the transmitted signal). For example, the receivers aboard the Cyclone Global Navigation Satellite System (CYGNSS) are designed to gather reflections from radio signals emitted by global positioning system (GPS) satellites from water surfaces on Earth (Ruf et al. 2013). CYGNSS is a constellation of eight low-Earth-orbit small satellites with orbits designed to maximize coverage and sampling frequency between 38°N and 38°S latitude, ideal for monitoring TC development, intensification, and decay (Ruf et al. 2017). As in the case of radio occultation, the GPS radio signals penetrate clouds and precipitation, offering unique access to the near-surface environment of TCs.

While CYGNSS-derived near-surface wind speeds can be helpful for diagnosis and prognosis of weather over otherwise sparsely observed oceans, further information can be gathered by applying a two-dimensional variational method (VAM) to derive vector (i.e., directional) winds. Vector wind fields are important because they provide information about near-surface divergence, convergence, and vorticity. This method was pioneered by Hoffman (1982, 1984) in order to resolve the inherent wind-direction ambiguity in retrieved scatterometer winds by optimally combining scatterometer scalar wind retrievals with an a priori estimate of wind direction. The approach has been used to produce optimal wind field analyses (Leidner et al. 2018) and climatologies of surface wind speeds over sparsely observed oceans (Atlas et al. 1996, 2011).

The purpose of this study is to investigate the impact of CYGNSS-derived near-surface scalar and vector winds on TC forecasts in global and regional assimilation and forecast systems. To do this, we used a technique known as an observing system experiment (OSE), also commonly known as a data denial experiment. In an OSE, two types of tests are conducted: 1) a control test in which a common suite of observations is assimilated and 2) further experimental tests that add or remove the types of observations under study. To the authors' knowledge, the only study to date to attempt a similar analysis for CYGNSS looked at the impact of CYGNSS-derived scalar winds on Hurricanes Harvey and Irma in 2017 (Cui et al. 2019). That study used the regional Hurricane Weather Research and Forecasting (HWRF; Biswas et al. 2017) Model to produce 126-h forecasts from analyses optimized using the Gridpoint Statistical Interpolation (GSI) hybrid ensemble three-dimensional variational data assimilation system (3DEnVar). When CYGNSS observations were added to a control test, improvements were found in 38% of Harvey track, maximum wind speed V_{max}, and minimum sea level pressure (MSLP) forecasts. Irma forecasts were improved 48% of the time for track, 37% of the time for V_{max}, and 44% of the time for MSLP. Modest improvements in the TC core structure were also found for some forecast lead times, especially through better portrayal of vortex circulation asymmetries.

In addition, prior to the launch of CYGNSS, several studies investigated the impact of simulated CYGNSS-derived winds using regional observing system simulation experiments (OSSEs; McNoldy et al. 2017; Zhang et al. 2017; Annane et al. 2018; Leidner et al. 2018). An OSSE is based on the same principle as an OSE, but uses observations derived from a simulated atmosphere to test observations that are not yet available (e.g., Hoffman and Atlas 2016). The four CYGNSS OSSE studies previously cited used a regional OSSE system in which the HWRF limited-area model was used to produce TC forecasts using the simulated observations. McNoldy et al. (2017) and Zhang et al. (2017) studied the impact of scalar winds and found some improvements in analyses and forecasts of track, V_{max}, and storm structure. McNoldy et al. (2017) suggested that adding a directional component may provide further improvements. Annane et al. (2018) found positive impacts for both scalar and vector winds, especially when cycling every 3 h as compared with 1- or 6-h cycling. Leidner et al. (2018) found more consistent improvement in V_{max} (~2–5 kt) than track forecasts, with vector winds more helpful than scalar winds for the representation of surface wind field structures. Without the directional wind components, analyses were more susceptible to dynamic imbalances and storm structure asymmetries.

The present study differs from previous similar studies in that it conducted data impact tests in the context of a global OSE and with a larger forecast sample size. CYGNSS-derived scalar and vector winds were assimilated into an experimental-resolution version of the National Centers for Environmental Prediction (NCEP) operational global analysis and forecasting system. In addition, the HWRF model was used to provide further high-resolution results. The HWRF analysis and forecast system used initial and lateral boundary conditions from the global analysis and forecasting system.

Section 2 describes the method used for this study, including details about the modeling and analysis system, CYGNSS data, and experiments. Global and regional model results are discussed in section 3. Main conclusions and future work are discussed in section 4.

2. Method

a. *Atmospheric modeling and analysis system*

This study was conducted by running week-long global forecasts using an experimental version of NCEP's Global Forecast System with Finite-Volume Cubed-Sphere dynamical core (FV3-GFS). Forecasts were initialized with analyses generated using the GSI within the Global Data Assimilation System (GDAS). The GSI employed a hybrid ensemble four-dimensional variational assimilation method (4DEnVar), which generated background error estimates using a 20-member ensemble forecast. Analyses were generated at 0000, 0600, 1200, and 1800 UTC each day from 15 September to 15 October 2018. Assimilation cycles in September were used for model spinup.

Global forecasts were initialized at 0000 UTC each day from 1 October to 15 October and run for 168 h. Producing only one forecast per day was done to avoid the issue of serial correlation since forecasts tend to be correlated with prior forecasts (Aberson and DeMaria 1994).

Observations were assimilated in 6-h windows centered on the analysis time (±3 h). All observations assimilated in the operational configuration (i.e., temperature, moisture, pressure, u wind, v wind, radio occultation, and satellite radiances) were also assimilated in our experiment. CYGNSS-derived scalar winds were assimilated using a preexisting forward operator designed for wind speed. CYGNSS- and VAM-derived vector winds were assimilated using a preexisting forward operator designed for wind reports from ships. The forward operator for wind speed assigned the observation height at 20 m above the surface, which represents a small incompatibility with CYGNSS-derived wind data, which are generally treated as 10-m winds. The forward operator for vector winds used the observation height of 10 m.

The experimental versions of the FV3-GFS and GDAS used in this study were of lower resolution than the operational configuration. The FV3 core configures forecast output into a cube with six equal sides; the resolution is denoted by the letter C, followed by the number of horizontal and vertical grid points on each face of the cube. Specifically, the experimental FV3-GFS used in this study was of C384 resolution (384 × 384 grid points on each cube face; ~27-km horizontal spacing) and the 20-member ensemble forecasts in the GDAS were of C192 resolution (~50-km horizontal spacing). In comparison, the operational FV3-GFS in November 2019 was of C768 (~13-km horizontal spacing) and the 80-member ensemble forecasts in the GDAS were of C384 (~27-km horizontal spacing). Both experimental and operational models used the same 65 vertical levels. The lower resolution in the global model reduced its ability to accurately reproduce the V_{max} of a strong TC but should not greatly impact the accuracy of track forecasts (e.g., Mueller et al. 2020).

To address the resolution challenge, we used the operational-resolution HWRF Model to simulate Hurricane Michael during its developmental phase using the experimental-resolution FV3-GFS output for lateral boundary and initial conditions. We used the H219 version of the HWRF system (Biswas et al. 2018). The HWRF was composed of three domains: 1) a fixed 77.2° × 77.2° parent domain with 13.5-km grid spacing, 2) a vortex-following 17.8° × 17.8° middle domain with 4.5-km grid spacing, and 3) a vortex-following 5.9° × 5.9° inner domain with 1.5-km grid spacing. Although the parent domain was fixed during a given forecast, its location was updated at each cycle to better capture the large-scale features surrounding the TC. On the other hand, the two nested domains were centered on the TC vortex and therefore moved during the forecasts. There were 75 vertical levels with a 10-hPa model top for each domain. Comprehensive details about the H219 system can be found in Biswas et al. (2018).

b. CYGNSS data and processing

The raw scattered GPS radio signals collected by CYGNSS receivers are first transformed into the Level-1 observables normalized bistatic radar cross section and leading-edge slope (Gleason et al. 2016, 2019). These Level-1 quantities are used to retrieve the Level-2 estimates of 10-m winds (Clarizia and Ruf 2016b). The geophysical model functions (GMFs; Ruf and Balasubramaniam 2019) used to map between Level-1 and Level-2 data are different for two sea states: fully developed seas (FDS; characterized by mature periodic waves without rapid changes in wind or sea state) and young seas with limited fetch (YSLF; characterized by rapidly changing wind and sea state, more common near stormy weather). We chose to use winds retrieved using the FDS algorithm since 1) FDS conditions prevail over much of the global ocean surface and 2) high-wind areas typical of YSLF conditions currently make retrievals difficult. The CYGNSS version-2.1 Level-2 data used in this study were obtained through the Jet Propulsion Laboratory's Physical Oceanography Distributed Active Archive Center (PODAAC; https://podaac.jpl.nasa.gov/dataset/CYGNSS_L2_V2.1). Figure 1 shows the progression of CYGNSS coverage for three assimilation cycles.

A limiting factor for the utility of CYGNSS data is that the relationship between surface roughness and wind speed becomes more complex at higher wind speed and surface roughness thresholds. For example, GMFs clearly map between surface roughness and wind speed while wind speeds are below 15–20 m s^{-1} (Ruf et al. 2019). At higher wind speeds, small changes in surface roughness map to larger ranges of wind speed estimates; therefore, higher derived wind speeds are more uncertain and may not be appropriate for assimilation in this study. Further, there are well-documented negative biases in CYGNSS retrieved wind speeds > 15 m s^{-1} resulting from the complex sea states produced by high winds and the localized nature of such winds. As a result, we discarded all CYGNSS observations > 15 m s^{-1}. With the exclusive use of lower wind speeds, the modulation of reflection by nonlocal swells can be an issue; however, addressing this issue is an area of active scientific research and lies outside the scope of this study.

A further challenge to assimilating CYGNSS data originates in the spatial density of measurements. Each CYGNSS observation is represented at the point of maximum reflection on the ocean surface (i.e., the specular point); however, the received signal does not come exclusively from the specular point, but from an elliptical area surrounding the specular point that is 25–35 km along the major axis, depending on incidence angle (Clarizia and Ruf 2016a,b). The challenge comes from the fact that observations are collected about every 6 km along the specular path. This leads to considerable overlap in successive observations (i.e., adjacent observations sample much of the same ocean surface area only seconds apart, leading to correlation between the observations). Using all these observations without any adjustments risks overfitting the model state to the observations.

To overcome this issue, we inflated observation errors to lessen the impact of individual observations on the analysis. Alternatives such as a priori data thinning or superobbing could be used in subsequent studies. Instead, we ingested all observations, but inflated observation errors by a factor of 5 to account for observation correlation and the mismatch between the high-resolution dataset and the lower-resolution data

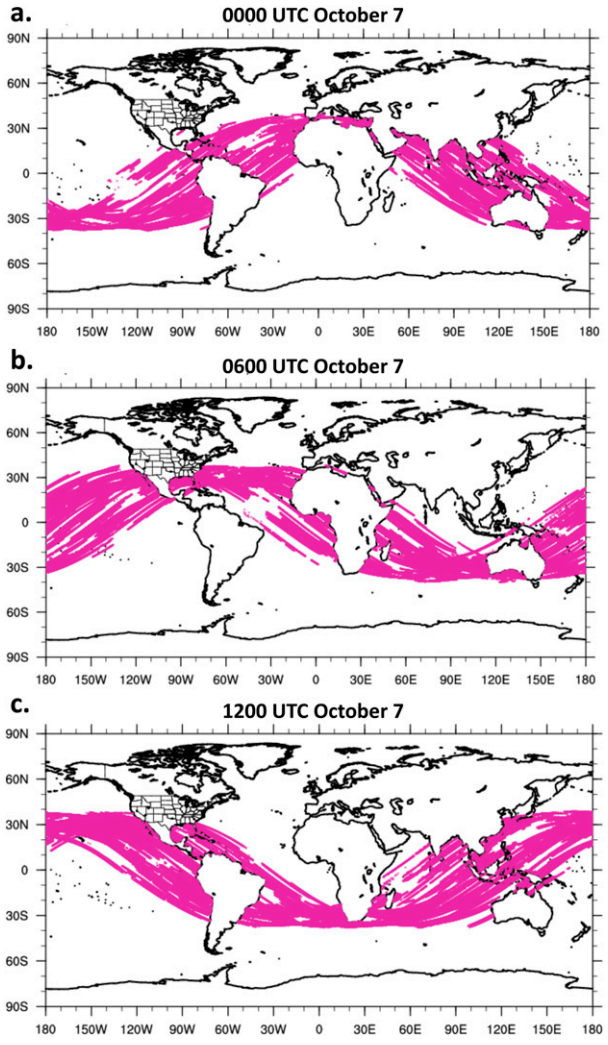

FIG. 1. Progression of CYGNSS coverage for three successive analysis times: (a) 0000 UTC 7 Oct, (b) 0600 UTC 7 Oct, and (c) 1200 UTC 7 Oct. Assimilation windows are ±3 h centered on the respective analysis times. Individual points represent observations at specular points. Because of the scale of the plots, dots appear to form lines, which are known as specular point tracks.

assimilation system (i.e., representativeness error). The inflation factor was the result of sensitivity tests that compared the root-mean square (RMS) error of post-analysis residuals (observation minus analyses) from VAM analyses using thinned data (independent samples) with VAM analyses that fit all of the data (no thinning; correlated observations) with inflated observation errors. The RMS post-analysis residuals using thinned and not-thinned CYGNSS retrievals were equivalent when the observation error used for the not-thinned data were 5 times as large. Because the observation gross error quality-control algorithm in GSI was impacted by the supplied observation error, the rejection thresholds for CYGNSS were adjusted to accommodate the increased observation error and to roughly match the rejection rate of other ocean surface wind data types (i.e., typically 1%–5%).

c. *VAM details*

Since this study investigated the impact of CYGNSS-derived vector winds in addition to scalar winds, we implemented a two-dimensional VAM to derive a vector wind field. The VAM created the vector wind field by optimizing the combination of Level-2 scalar winds and an a priori wind vector field. The wind field was then interpolated to the CYGNSS specular point locations. Hoffman et al. (2003) provides an in-depth description of this method.

In this study, the a priori wind fields used with the VAM were analyses from the operational GFS. At the time of the experiment (September–October 2018), the operational GFS used the Global Spectral Model (GSM) core. Since the GSM and the FV3 used in this study are different dynamical cores, we deemed that the GSM wind field was independent from the FV3 state.

d. *Experimental design*

To investigate the impact of CYGNSS-derived wind observations on TC forecasts, we conducted three main tests in the global modeling system that 1) assimilated all operationally assimilated observations (CTL), 2) assimilated control observations plus CYGNSS-derived near-surface scalar winds (CYGSPD), and 3) assimilated control observations plus CYGNSS-derived near-surface VAM vector winds (CYGDIR). CTL and CYGSPD were supplemented with higher-resolution HWRF forecasts using the global forecasts as the source for HWRF initial conditions and lateral boundary conditions. CYGNSS data were not assimilated directly in HWRF in these supplemental tests. These tests are referred to as HWRF_CTL and HWRF_SPD, respectively.

e. *Verification*

Forecast verification was based on best-track data from the NHC HURDAT-2 database (Landsea and Franklin 2013) and the JTWC database (Chu et al. 2002). The TCs used are Leslie, Michael, and Nadine in the North Atlantic Ocean; Rosa, Sergio, and Tara in the eastern Pacific Ocean; and Kong-Rey in the western Pacific (Fig. 2). All TCs were from October 2018. These best-track data represented TC location in increments of 0.1° latitude–longitude, V_{max} in increments of 5 kt, and MSLP in increments of 1 hPa.

Data for global forecast verification came from the Geophysical Fluid Dynamics Laboratory's (GFDL) vortex tracker embedded within the FV3-GFS and GDAS experimental system. The tracker was applied to the 0.25° × 0.25° (~27 km) forecast output grid. Known existing TCs were tracked using TC Vitals files included in the experimental system and used in operations. Data for regional model verification came from the GFDL vortex tracker applied to a regridded version of the parent 13.5-km domain. The GFDL vortex tracker provided TC location in increments of 0.1° latitude and longitude, V_{max} in increments of 1 kt, and MSLP in increments of 1 hPa for both global and regional model forecasts.

Verification metrics presented in this study were track, V_{max}, and MSLP errors. MSLP errors were presented for HWRF results only. To determine whether global CYGSPD or CYGDIR impacts were statistically significant, we used a paired t test with 95% confidence intervals (Hamill 1999; Gilleland et al. 2018). Any averaged difference (with respect to CTL) that fell outside

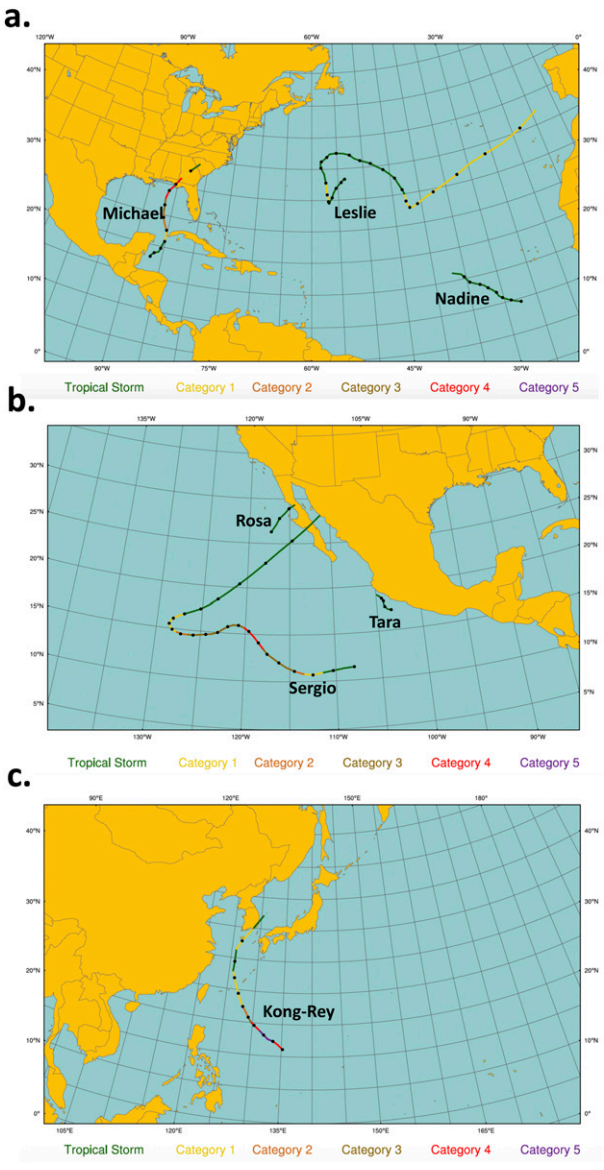

FIG. 2. Storm track (lines) and intensity category (colors) for TCs investigated in the study in the (a) North Atlantic, (b) eastern Pacific, and (c) western Pacific basins; TC tracks are shown only after 1 Oct 2018 (investigation period) and do not include tracks from September. Data are obtained from HURDAT-2 (for Atlantic and eastern Pacific basins) and JTWC (for western Pacific basin) databases. Black dots denote TC center location at 0000 and 1200 UTC every day.

these intervals was statistically significant. The sample size of HWRF Hurricane Michael forecasts (six forecasts) was insufficient to assign statistical significance.

3. OSE results

a. *Assimilation statistics*

Observation-minus-background (labeled o-b) and observation-minus-analysis (labeled o-a) statistics for CYGNSS-derived observations were compared with those of the Advanced Scatterometer (ASCAT) for every cycle from 15 September to 15 October 2018. ASCAT is another instrument that determines wind speed and direction using electromagnetic backscatter from water surfaces and those data are ingested during operations using an established forward operator. By comparing CYGNSS assimilation with ASCAT assimilation in both CYGSPD and CYGDIR, we assessed whether the observation operators, inflated observation errors, and adjusted gross error checks were working to assimilate CYGNSS data reasonably.

Assimilated observation counts per cycle for ASCAT during this period were ~15 000–20 000 between *MetOp-A* and *MetOp-B* satellites and from 130 000 to 250 000 for CYGNSS. Rejection rates for ASCAT decreased from ~3% relative to the background to 1.5% relative to the analysis in both CYGSPD and CYGDIR tests, while CYGNSS rejection rates decreased from 1.5% to 0.5% in CYGSPD and from 0.75% to 0.25% in CYGDIR (Figs. 3a,d). The lower rejection rates for CYGNSS data were primarily because the winds were restricted to $\leq 15\,\mathrm{m\,s^{-1}}$, and weaker winds had a lower overall rejection rate than the full spectrum of ocean wind speeds represented in the ASCAT data. Bias statistics also showed decreases from o-b to o-a, with ASCAT decreasing from 0.2 to $0.15\,\mathrm{m\,s^{-1}}$ in both tests, while CYGNSS decreased from 0.35 to $0.25\,\mathrm{m\,s^{-1}}$ in CYGSPD and from 0.3 to $0.15\,\mathrm{m\,s^{-1}}$ in CYGDIR (Figs. 3b,e). ASCAT RMS error statistics showed decreases from 1.9 to $1.2\,\mathrm{m\,s^{-1}}$ in both tests, whereas CYGNSS RMS error decreased from 1.75 to $1.4\,\mathrm{m\,s^{-1}}$ in CYGSPD and from 1.5 to $1.05\,\mathrm{m\,s^{-1}}$ in CYGDIR (Figs. 3c,f). As with the rejection rate, the lower overall RMS error of CYGNSS innovation and residual statistics relative to ASCAT partially was a result of the elimination of CYGNSS winds $\geq 15\,\mathrm{m\,s^{-1}}$. These statistics were averages over all cycles, and both ASCAT and CYGNSS sometimes exhibited large cycle-to-cycle variability, most likely due to changes in global sampling from the nodal precession of ASCAT and CYGNSS orbits and the variability of observed weather patterns. While such variability was generally larger for CYGNSS observations, o-b bias and RMS error were reduced for every cycle for both CYGNSS and ASCAT observations.

b. *Global forecast impacts*

Globally averaged results showed that assimilating CYGNSS-derived near-surface wind speed produced very small ~5-km (not statistically significant) improvements in initial position at 0 h (Figs. 4a,b). Average (statistically significant) improvements of 20–40 km were evident by 36–54 h. After 60 h, no track results were statistically significant, with degradations from 96 to 108 h. The V_{max} forecast impacts were not statistically significant, except for a significant ~2-kt degradation at 6 h (Figs. 4c,d). After the first 24 h, impacts were generally less than 2 kt, with improvements common after 108 h.

Vector wind assimilation yielded slightly better results for track forecasts at longer lead times (Figs. 5a,b). Perhaps the largest difference relative to CYGSPD impact was that CYGDIR average track errors were less than CTL after 96 h. Other than significant improvements at 36 and 54 h, impacts (mainly improvements) were not statistically significant. Consistent 60–100-km improvements were found after 120 h, with forecast sample sizes

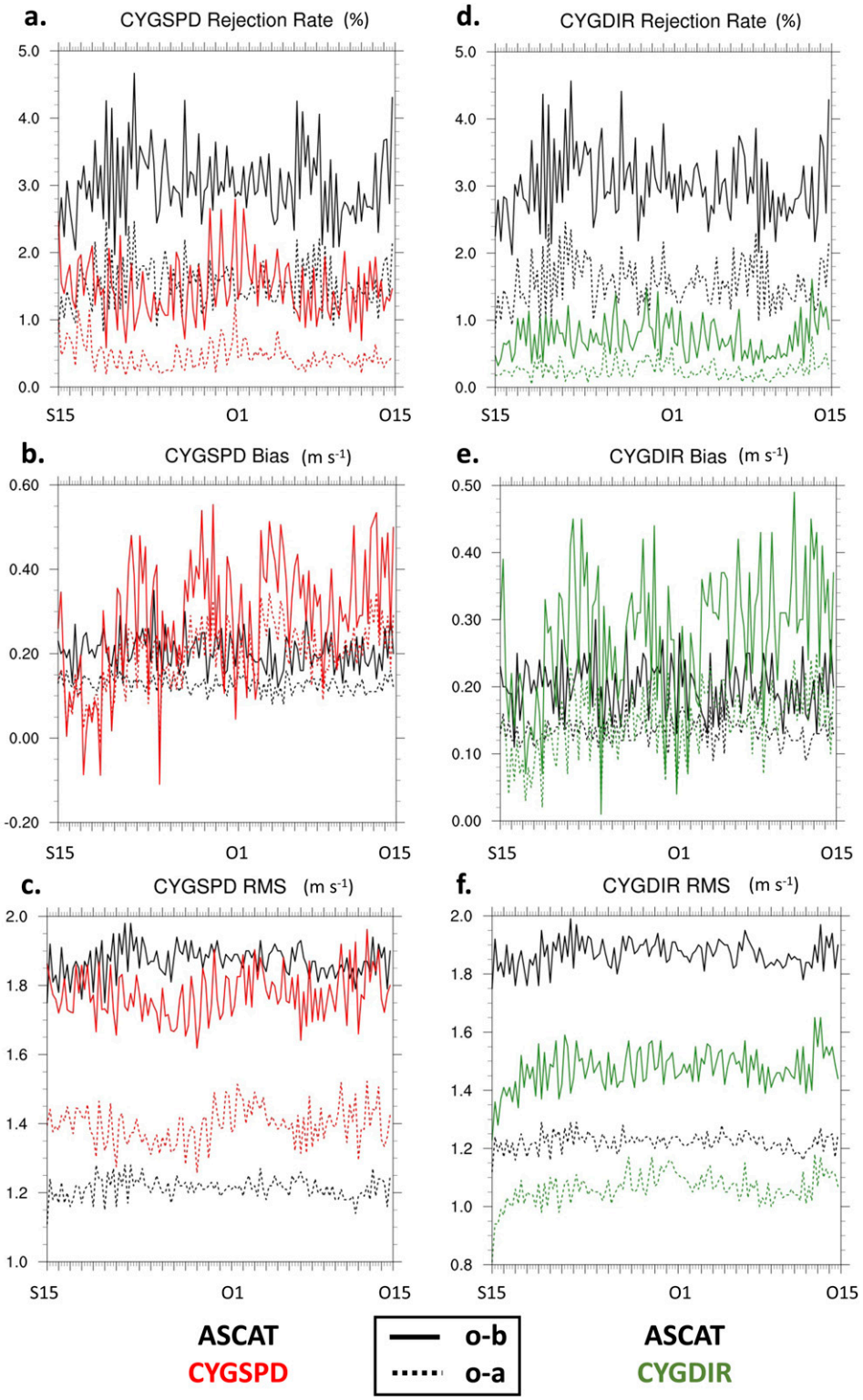

FIG. 3. Statistics for every assimilation cycle for ASCAT (black lines), (left) CYGSPD (red lines), and (right) CYGDIR (green lines) wind retrievals: (a),(d) observation rejection rate; (b),(e) bias; and (c),(f) rms error. Solid lines denote o-b statistics, and dashed lines denote o-a statistics (repeated in the left and right columns).

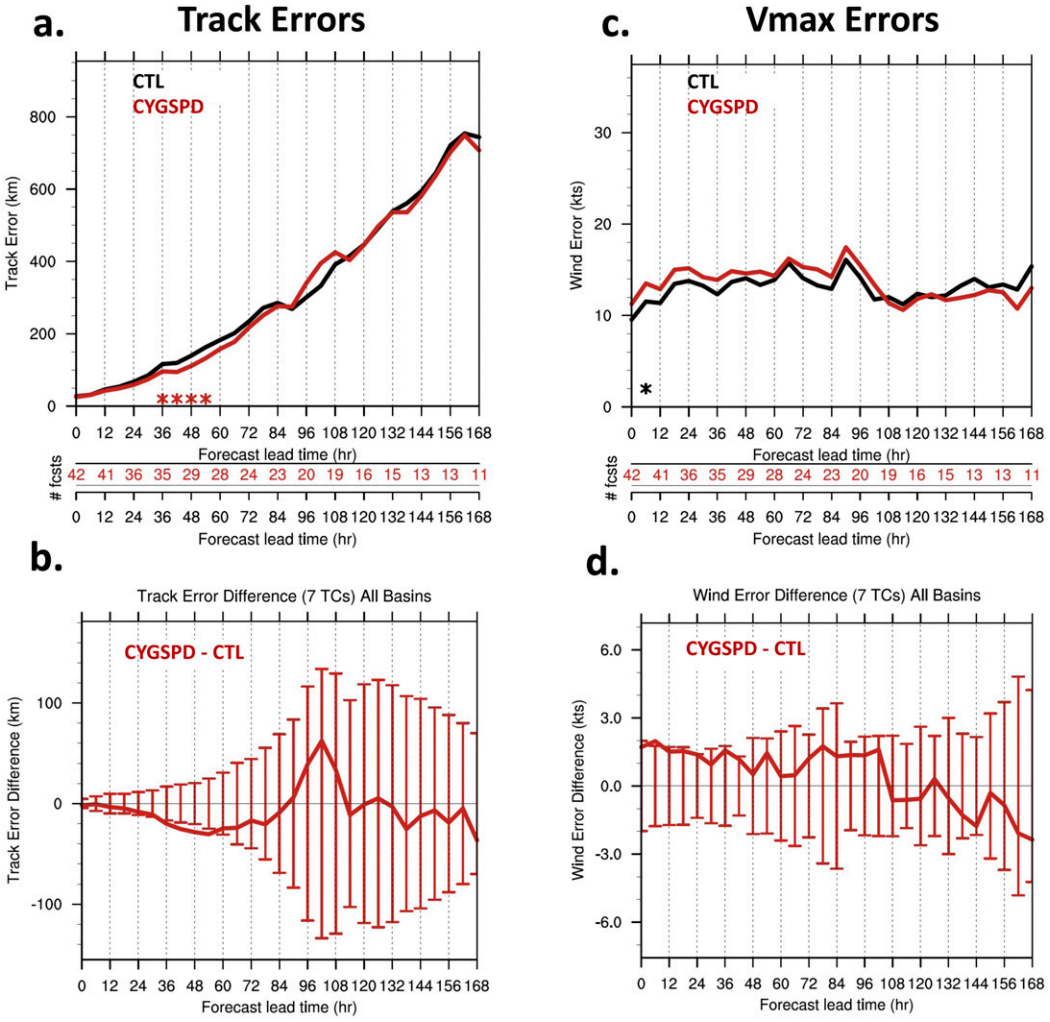

FIG. 4. Average forecast (top) error and (bottom) error difference statistics for (a),(b) track and (c),(d) V_{max}. Black lines denote CTL, and red lines denote CYGSPD. Asterisks denote statistically significant differences. Average error differences (CYGSPD − CTL) in (b) and (d) are shown with 95% confidence interval bars. Forecast sample size is also shown at each forecast lead time.

from 11 to 16. The V_{max} impacts were also not statistically significant except for ~2-kt statistically significant degradations at 0, 6, 24, and 72 h (Figs. 5c,d). The remainder of lead times had impacts of ≤2 kt with an equal mix of improvements and degradations.

Although there were some notable impacts in CYGSPD for individual TCs (Fig. 6), most impacts were small for most TCs over most lead times. Among the notable impacts were large 200–500-km degradations for Kong-Rey track forecasts (mainly from the along-track error component) after 78-h lead time and large 150–300-km improvements for Tropical Storm Nadine track forecasts (mainly from the cross-track error component) after 42-h lead time (Figs. 6a,b). A notable V_{max} impact was 10–20-kt degradation for Hurricane Michael, especially for 48–84-h lead times (Fig. 6c). The source of this degradation was one forecast, initialized 0000 UTC 7 October, that is examined in-depth in the next section. Note that the sample sizes for most individual storms were very small, so statistical significance was not calculated for single-storm investigations.

Individual storm statistics for CYGDIR were similar with some exceptions (Fig. 7). Hurricane Michael track forecasts were degraded by 50–70 km from 72 to 84 h (Fig. 7a) and V_{max} forecasts were not degraded from 48 to 72 h (Fig. 7b). Conversely, Tropical Storm Nadine and Hurricane Sergio track forecasts were improved over all lead times (Figs. 7c,d).

c. *Hurricane Michael: Global model*

Hurricane Michael was the first category-5 hurricane to make landfall in the continental United States since Hurricane Andrew in 1992. After developing as a tropical low in the western Caribbean Sea, this storm underwent rapid intensification as it moved northward through the eastern Gulf of Mexico. The extreme impact of this storm to life and property along the U.S. Gulf Coast and the impact of CYGNSS-derived

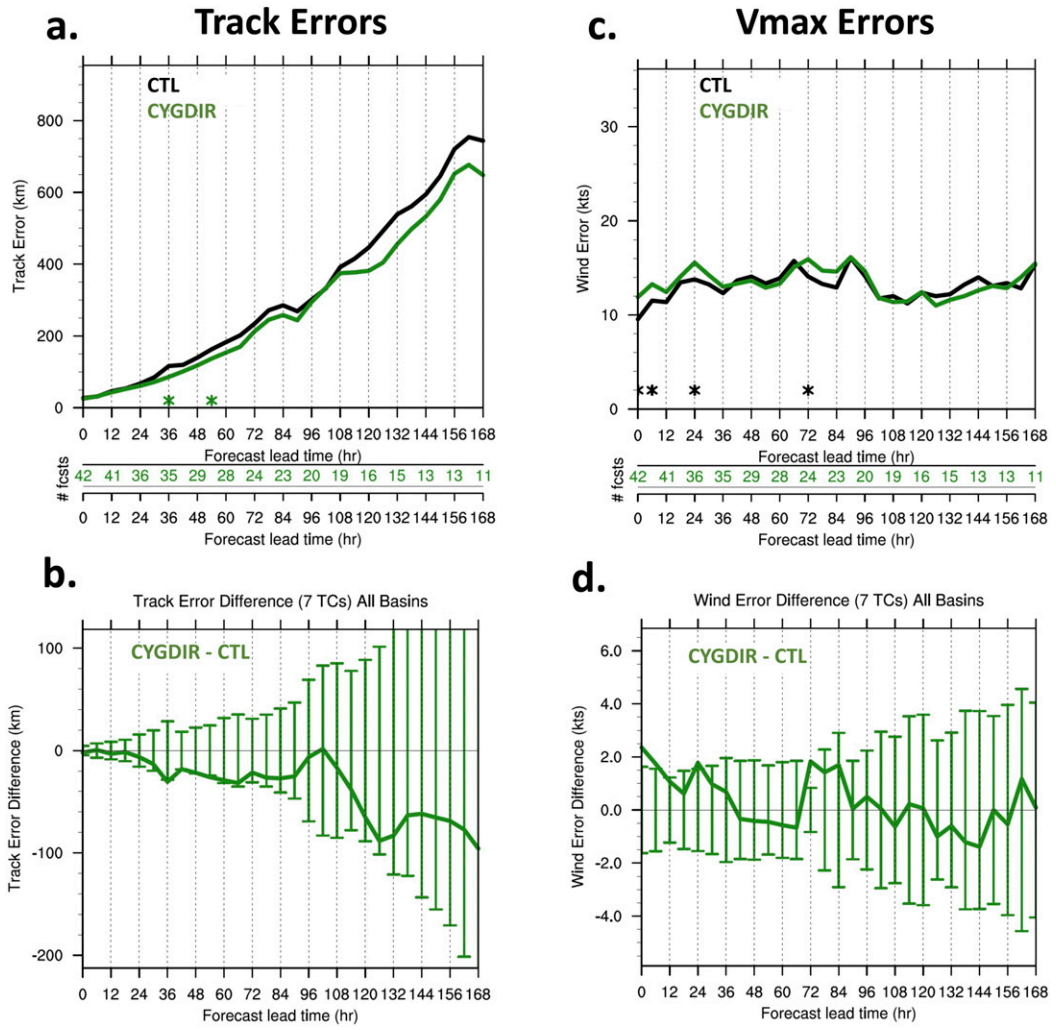

FIG. 5. As in Fig. 4, but for CTL (black lines) and CYGDIR (green lines).

near-surface wind speed on V_{max} forecasts made it an outstanding candidate for more in-depth study.

There were four GFS forecasts generated with initial times prior to Michael's landfall. These forecasts were initialized at 0000 UTC 7–10 October. In 8–10 October V_{max} forecasts, all three tests (CTL, CYGSPD, and CYGDIR) were similar at most lead times with some improvements in CYGNSS tests prior to landfall (Fig. 8). The most striking result was the degradation in CYGSPD for the 7 October forecast from 48- to 84-h lead time. The magnitude of the degradation was 20–40 kt, with maximum degradation just prior to landfall in the model even though CYGSPD V_{max} was more accurate than CTL and CYGDIR at initialization time.

A closer look at the track and V_{max} forecasts initialized at 0000 UTC 7 October at the 42-, 48-, and 78-h lead times revealed similar tracks for all three tests and a much weaker storm in CYGSPD (Fig. 9). All three tests resulted in landfall on the Florida panhandle at ~84-h lead time, albeit farther west than the best-track landfall. The storm's greatest intensification occurred between 42- and 48-h lead times in CTL and CYGDIR, but did not occur in CYGSPD. While all three tests had similar V_{max} at 42 h, the wind field for CYGSPD was much less symmetrical with V_{max} located more than 100 km northeast of the center (Fig. 9b). Furthermore, the CYGSPD MSLP was located slightly to the west of the storm track center location. Since the tracker used pressure and geopotential height fields at multiple levels, this suggests a disorganized storm that was not vertically stacked in the model representation. In contrast, both CTL and CYGDIR produced compact wind fields and MSLP collocated with the tracker centers.

By 48 h, both CTL and CYGDIR were positioned to begin more rapid intensification, while CYGSPD produced a storm that was still disorganized with an asymmetrical wind field and MSLP displaced from the tracker-identified center (Figs. 9d–f). At this time, all three model depictions showed that Michael had emerged into the eastern Gulf of Mexico, away from any possible interaction with land (i.e., Cuba) that might inhibit intensification. By 78 h, all three forecasts were approaching

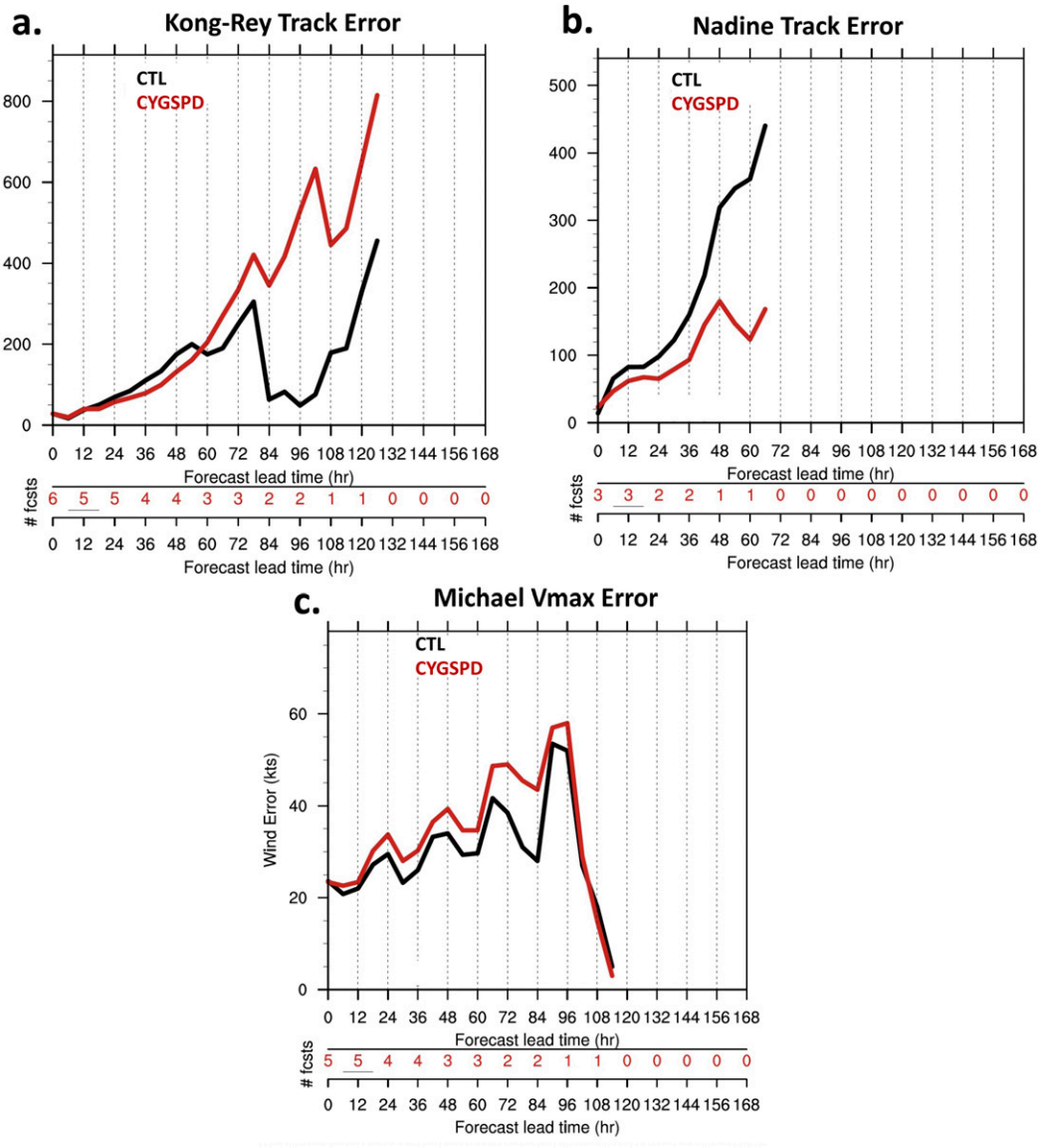

FIG. 6. Average track errors for (a) Kong-Rey and (b) Nadine and (c) average V_{max} errors for Michael for CTL (black) and CYGSPD (red) tests.

maximum V_{max} just prior to landfall (Figs. 9g–i). While CYGSPD produced a somewhat stronger and more organized storm than at 48 h, it did not recover from earlier degradations and consequently did not attain hurricane strength prior to landfall. Both CTL and CYGDIR produced hurricanes with V_{max} in the eastern two quadrants of the storm.

For observations located within the Fig. 9 field of view, assimilation of CYGNSS observations reduced the gap between observation and model from background to analysis at 69% of observation locations in CYGSPD and 68.7% of locations in CYGDIR. This is as compared with 71.1% reduced for CYGSPD and 68.2% reduced for CYGDIR globally, suggesting that CYGDIR assimilation was not negatively impacted near the developing low pressure. CYGSPD bias reduction was successful at slightly fewer observation locations near Michael than globally.

d. *Hurricane Michael: Regional model*

In addition to global models such as GFS, regional hurricane-specific models like the HWRF model are frequently used by the tropical cyclone forecasting community, especially for intensity forecasts. Thus, the potential benefit of CYGNSS assimilation into the global model is likely to be realized through the impact on HWRF forecasts via initial conditions (ICs) and lateral boundary conditions (LBCs). Thus, we used the CTL and CYGSPD tests as the source for HWRF ICs and LBCs for six 120-h forecasts of Hurricane Michael (initialized 0000 UTC 7 October 2018–0600 UTC 8 October 2018). The TC vortex

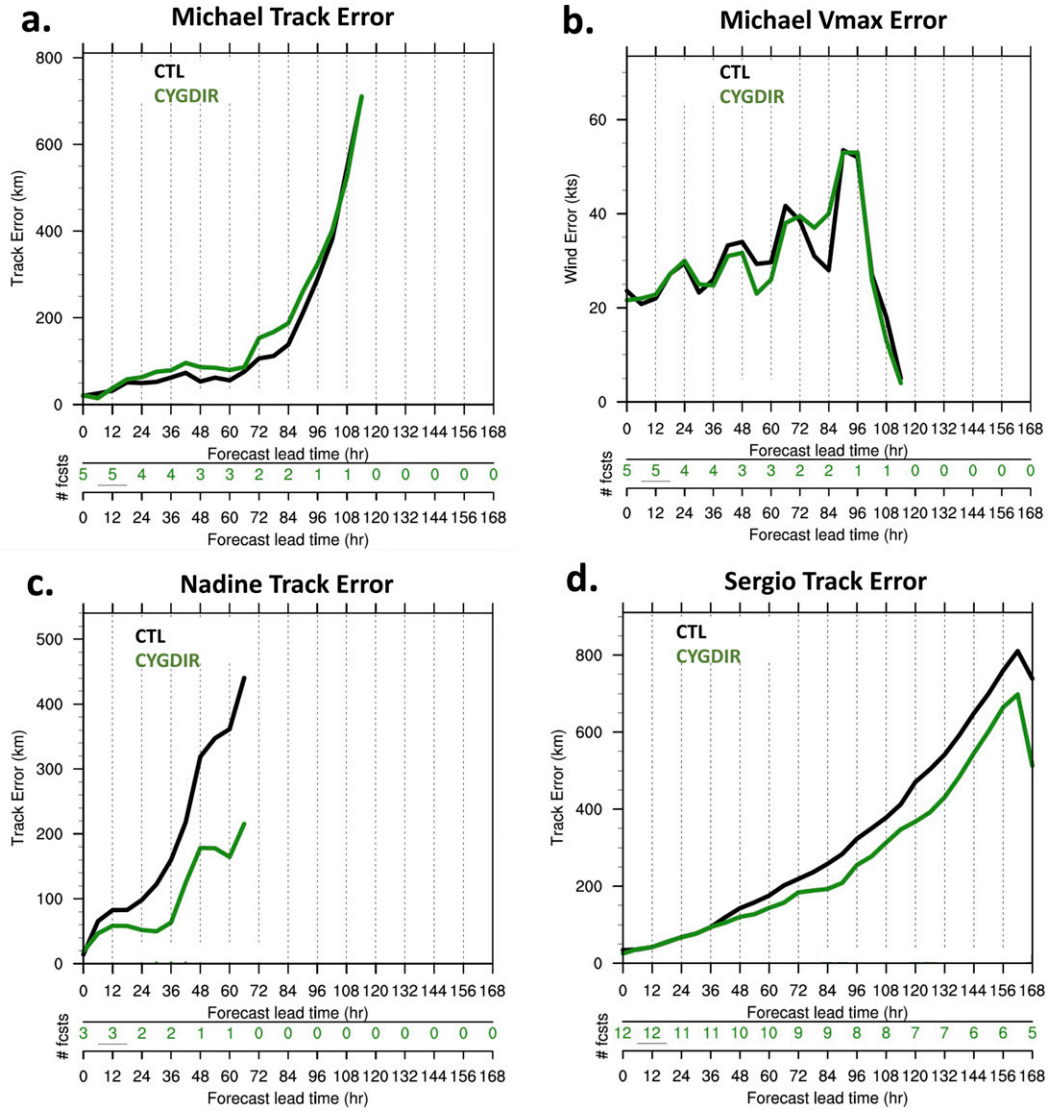

FIG. 7. Average (a) track errors for Michael, (b) V_{max} errors for Michael, (c) track errors for Nadine, and (d) track errors for Sergio for CTL (black) and CYGDIR (green) tests.

decayed after 96 h and could not be tracked, so plots show the first 96 h only. These forecasts covered the development and strengthening phase of a storm that experienced rapid intensification. Furthermore, the global CYGSPD test produced a notable lack of rapid intensification, leading to degraded V_{max} forecasts, as discussed before. These factors guided the choice of these cycles for the HWRF tests.

Track forecasts improved at every lead time after 0 h, reaching a maximum at 24 h with approximately 40 n mi (75 km) improvements (Fig. 10a). Improvements reduced to 5–10 n mi (9–18 km) by 72 h. The V_{max} and MSLP impacts were similar to each other, as expected given the dynamic relationship between central pressure and V_{max} (Figs. 10b,c). In the first 36 h, impacts were mainly improvements within 2 hPa and 4 kt. From 42 h through landfall, the improvements increased substantially to ~18 hPa and 22 kt for MSLP and V_{max}, respectively. The HWRF results with CYGNSS-influenced LBCs and ICs were far more promising than those from the GFS alone.

4. Conclusions

In this study, we used NCEP's Global Data Assimilation System and Global Forecast System in conjunction with the Hurricane Weather Research and Forecasting Model to investigate the impact of CYGNSS-derived scalar (CYGSPD) and vector (CYGDIR) near-surface winds on TC track and intensity forecasts. The GFS version used in this study incorporated the Finite-Volume Cubed-Sphere Dynamical Core (FV3-GFS), a choice that was meant to reflect the configuration of the GFS as of November 2019. The first 15 days of the

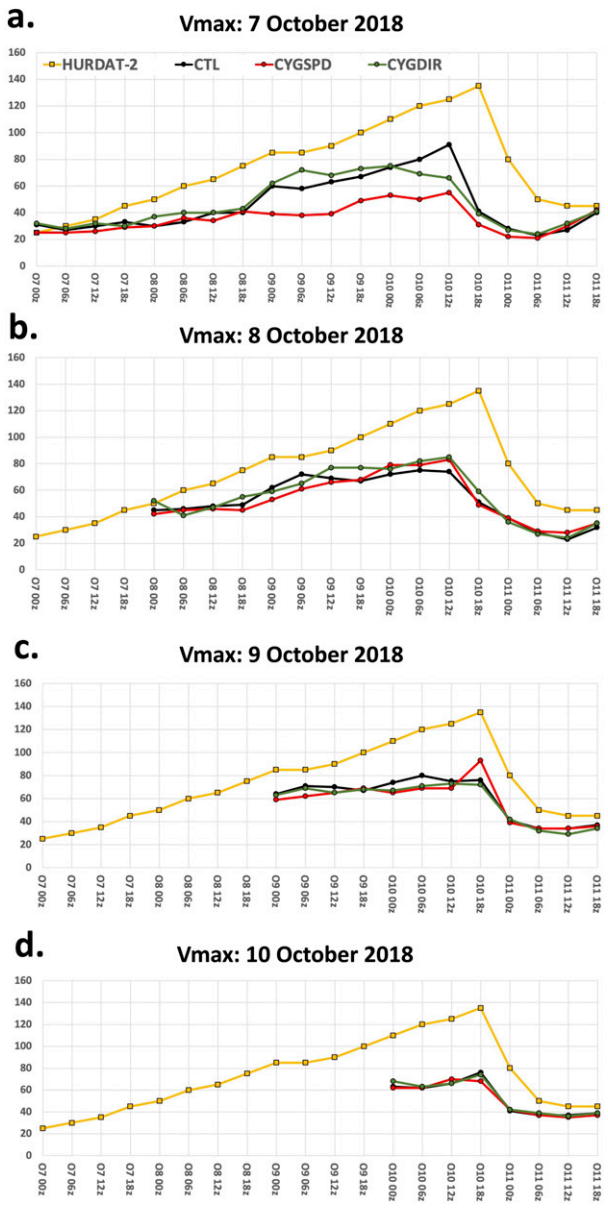

FIG. 8. Time series for Hurricane Michael V_{max} forecasts initialized at 0000 UTC (a) 7 Oct, (b) 8 Oct, (c) 9 Oct, and (d) 10 Oct for best track (yellow), CTL (black), CYGSPD (red), and CYGDIR (green).

experimental period (15 September–30 September 2018) were used to spin up the model state with the CYGNSS observations. The following 15 days (1 October–15 October 2018) were used to produce TC forecasts.

All observational data in the GDAS/GFS was assimilated via the hybrid four-dimensional ensemble variational technique (4DEnVar), the assimilation method employed in operations during the experimental period. Observations were assimilated in 6-h windows centered on four daily analysis times (0000, 0600, 1200, and 1800 UTC). Week-long GFS forecasts were initialized at 0000 UTC each day to avoid forecast error serial correlation. The GFS forecasts were used to provide ICs and LBCs for HWRF forecasts initialized every 6 h from 0000 UTC 7 October to 0600 UTC 8 October for Hurricane Michael. Additional GFS forecasts at 0600, 1200, and 1800 UTC were produced to accommodate the HWRF forecast cycle. The analysis of HWRF results included track, V_{max}, and MSLP.

This study found the following:

1) CYGNSS assimilation statistics were comparable to those of the Advanced Scatterometer, a similar instrument well established in operational assimilation cycles. Bias and root-mean-square error for both CYGNSS tests were shown to be reduced through assimilation by ratios similar to ASCAT. Additionally, CYGNSS cycle-to-cycle variability was larger than that for ASCAT. This suggests CYGNSS data were properly (although perhaps not optimally) assimilated in the global analysis system.
2) Global track and V_{max} forecasts were impacted at all lead times, although most results were not statistically significant. This is not surprising since there are already so many observations in the global observing system; however, track forecasts were statistically significantly improved in CYGSPD from 36- to 54-h lead time and in CYGDIR at 36- and 54-h lead times. The V_{max} impacts were even more subtle, with statistically significant ~2-kt degradations at one lead time in CYGSPD and four lead times in CYGDIR.
3) The impacts for most TC forecasts were mixed with some improvements and some degradations. The Hurricane Michael V_{max} forecasts initialized on 7 October revealed large 20–40-kt degradations in the CYGSPD global model test. This resulted from a lack of rapid intensification in the 2 days prior to landfall. This, in turn, was traced back to a lack of well-defined structure in the CYGSPD storm prior to the time when rapid intensification actually occurred.
4) HWRF forecasts based on ICs and LBCs from the CTL and CYGSPD tests showed modest improvements for track and dramatic improvements for intensity metrics MSLP and V_{max}, especially during the period of rapid intensification. The improvements in intensity metrics in the HWRF system relative to the global model system were not surprising given the intrinsic limitations of the global model's lower resolution and TC-specific strengths of HWRF model physics.

It is important to understand how these results fit within the context of previous attempts to improve TC forecasts by using CYGNSS data. As mentioned in section 1, previous OSSEs (Annane et al. 2018; Leidner et al. 2018) using HWRF found neutral impacts for tracks and some improvements (generally 5 kt or less) for V_{max} forecasts for single TC case studies. The previous OSE (Cui et al. 2019) also used HWRF but featured different metrics than this study. Its findings of generally neutral to positive impacts for track and V_{max} for two TC cases were promising. Similarly, the present study found improvements in track forecasts in both global and regional models and improvements in intensity metrics in the high-resolution regional model. The main difference between the results of this study and previous studies is the presence of neutral to negative impacts on V_{max} forecasts in the global model, which may

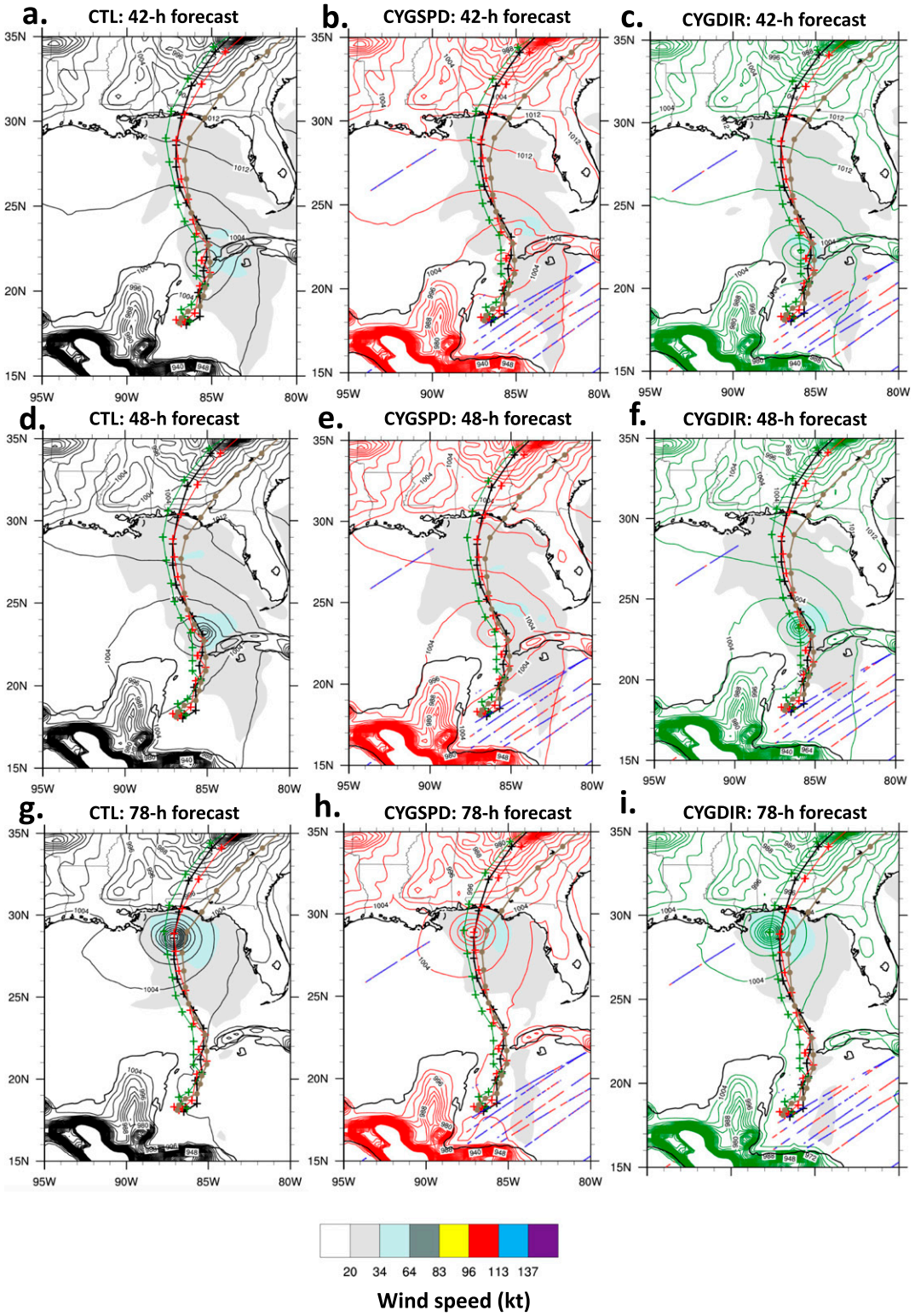

FIG. 9. Surface pressure and 10-m wind speed forecasts for (left) CTL, (center) CYGSPD, and (right) CYGDIR at (a)–(c) 42-, (d)–(f) 48-, and (g)–(i) 78-h lead times from the forecast initialized 0000 UTC 7 Oct 2018. Also plotted are best tracks (tan) and CTL (black), CYGSPD (red), and CYGDIR (green) track forecasts with symbols every 6 h. Assimilated CYGNSS observations are plotted with red dots (o-a larger than o-b) and blue dots (o-a smaller than o-b).

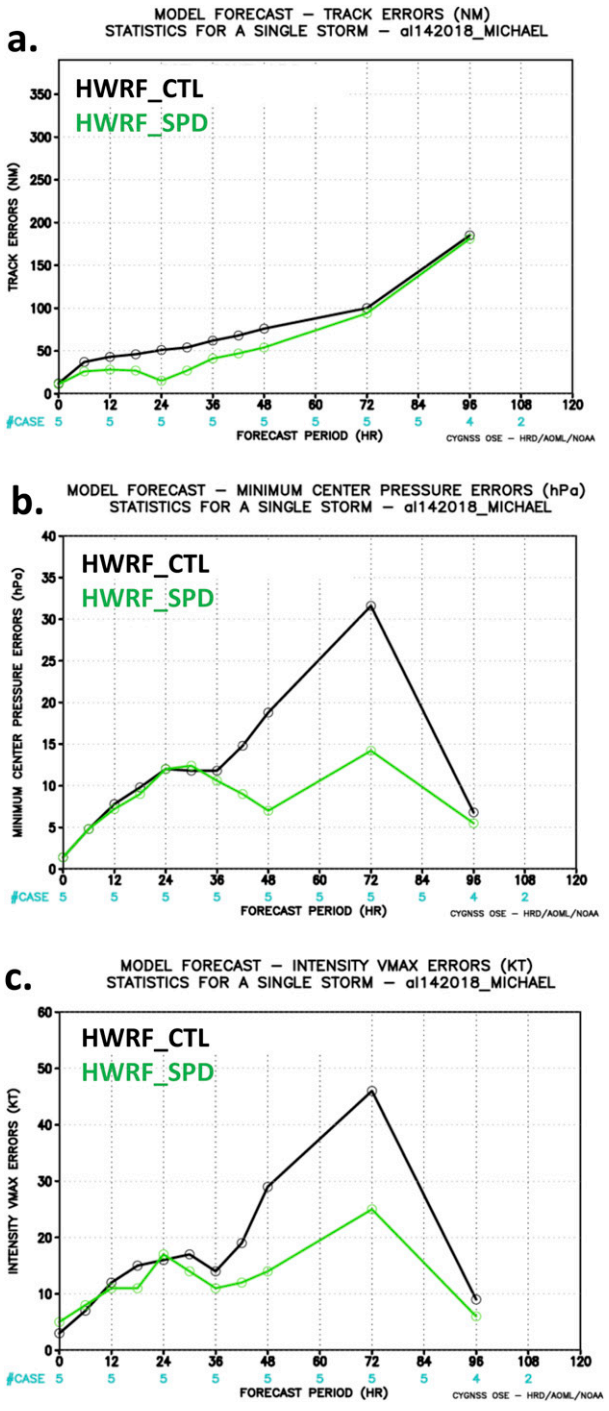

FIG. 10. Average HWRF error statistics for (a) track (in nautical miles), (b) MSLP, and (c) V_{max} for HWRF_CTL (black) and HWRF_SPD (green). Sample sizes shown in blue as $N - 1$, where N is number of forecasts.

be due to HWRF providing superior physical representation of the TC inner core by virtue of higher resolution and more appropriate model physics. Any direct comparisons between previous studies and this study should be considered with caution. Plenty of methodological differences exist between them, perhaps most importantly that previous studies assimilated CYGNSS data directly into the HWRF data assimilation system, while in this study CYGNSS was assimilated only in the global model with the impact on HWRF forecasts due to the influence of ICs and LBCs.

An important caveat for these conclusions is that the global modeling and analysis system was run at lower-than-operational resolution, which was most potentially detrimental for V_{max} forecasts. While track forecast impacts from the global model tests are likely reliable, caution is warranted for interpretation of V_{max} results. In addition to model representation of fields that require higher resolution, the physical development of these fields depend on small-scale dynamics and thermodynamics that may not be present in the model (Goldenberg et al. 2015). To help overcome this issue, we used the HWRF at operational resolution with global model ICs and LBCs, showing a much more promising outcome. A further caveat is that the gross error quality control parameters were tuned but not optimized for CYGNSS observations prior to running the tests. Preexisting observation operators were used to generate bias and spread statistics for four assimilation cycles. These statistics were compared with ASCAT statistics to arrive at gross error quality control check parameters empirically. Work on further optimizing gross error thresholds for CYGNSS data in the global system will be needed to fully realize the potential benefit of the data. The last caveat is that only wind speeds $\leq 15\,\mathrm{m\,s^{-1}}$ were assimilated.

As a new observing system, CYGNSS presented some challenges to the current study, including 1) characterizing observation error in the context of atmospheric data assimilation systems at very different resolutions (i.e., global vs nested regional); 2) accounting for serial correlation in the information content and errors present in the 1-Hz CYGNSS specular point tracks of retrieved winds; and 3) how to handle CYGNSS retrieved winds $> 15\,\mathrm{m\,s^{-1}}$, since the wind speed retrieval errors become very large at higher wind speeds. Future research should address the interplay of CYGNSS information between global and regional-scale models, devise a more fundamental treatment of CYGNSS observation error correlation within each specular point track, and find approaches to assimilate CYGNSS wind retrievals in environments with winds $> 15\,\mathrm{m\,s^{-1}}$.

Acknowledgments. The authors acknowledge Dr. Altug Aksoy and Mr. Stanley Goldenberg for their helpful comments and suggestions to improve the paper. Three anonymous reviewers also provided valuable feedback that led to the refinement and improvement of the paper. This research of the Atlantic Oceanographic and Meteorological Laboratory (AOML) is supported by NOAA's Climate Adaptation and Mitigation Program (CAMP) and administered by UCAR's Cooperative Programs for the Advancement of Earth System Science (CPAESS) under Awards NA18OAR4310253, NA18OAR4310253B, and NA18OAR4310253C.

Data availability statement. Model datasets are not publicly available, but they are on long-term storage and can be made available upon request.

REFERENCES

Aberson, S. D., and M. DeMaria, 1994: Verification of a nested barotropic hurricane track forecast model (VICBAR). *Mon. Wea. Rev.*, **122**, 2804–2815, https://doi.org/10.1175/1520-0493(1994)122<2804:VOANBH>2.0.CO;2.

Anisetty, S. K. A. V. P. R., C.-Y. Huang, and S.-Y. Chen, 2014: Impact of FORMOSAT-3/COSMIC radio occultation data on the prediction of super cyclone Gonu (2007): A case study. *Nat. Hazards*, **70**, 1209–1230, https://doi.org/10.1007/s11069-013-0870-0.

Annane, B., B. McNoldy, S. M. Leidner, R. Hoffman, R. Atlas, and S. J. Majumdar, 2018: A study of the HWRF analysis and forecast impact of realistically simulated CYGNSS observations assimilated as scalar wind speeds and as VAM wind vectors. *Mon. Wea. Rev.*, **146**, 2221–2236, https://doi.org/10.1175/MWR-D-17-0240.1.

Atlas, R., R. N. Hoffman, S. C. Bloom, J. C. Jusem, and J. Ardizzone, 1996: A multiyear global surface wind velocity dataset using SSM/I wind observations. *Bull. Amer. Meteor. Soc.*, **77**, 869–882, https://doi.org/10.1175/1520-0477(1996)077<0869:AMGSWV>2.0.CO;2.

——, ——, J. Ardizzone, S. M. Leidner, J. C. Jusem, D. K. Smith, and D. Gombos, 2011: A cross-calibrated, multiplatform ocean surface wind velocity product for meteorological and oceanographic applications. *Bull. Amer. Meteor. Soc.*, **92**, 157–174, https://doi.org/10.1175/2010BAMS2946.1.

Biswas, M. K., L. Carson, K. Newman, L. Bernardet, E. Kalina, and E. Grell, 2017: Community HWRF users' guide V3.9a. NOAA Tech. Memo. OAR GSD-51, 163 pp., https://doi.org/10.7289/V5/TM-OAR-GSD-51.

——, ——, ——, D. Stark, E. Kalina, E. Grell, and J. Frimel, 2018: Community HWRF users' guide V4.0a. Developmental Testbed Center, 163 pp., https://dtcenter.org/sites/default/files/community-code/hwrf/docs/users_guide/HWRF-UG-2018.pdf.

Chen, Y.-C., M.-E. Hsieh, L.-F. Hsiao, Y.-H. Kuo, M.-J. Yang, C.-Y. Huang, and C.-S. Lee, 2015: Systematic evaluation of the impacts of GPSRO data on the prediction of typhoons over the Northwestern Pacific in 2008–2010. *Atmos. Meas. Tech.*, **8**, 2531–2542, https://doi.org/10.5194/amt-8-2531-2015.

Chu, J.-H., C. R. Sampson, A. S. Levine, and E. Fukada, 2002: The Joint Typhoon Warning Center tropical cyclone best-tracks, 1945–2000. Naval Research Laboratory Rep. NRL/MR/7540-02-16, 22 pp.

Clarizia, M. P., and C. S. Ruf, 2016a: On the spatial resolution of GNSS-reflectometry. *IEEE Geosci. Remote Sens. Lett.*, **13**, 1064–1068, https://doi.org/10.1109/LGRS.2016.2565380.

——, and ——, 2016b: Wind speed retrieval algorithm for the Cyclone Global Navigation Satellite System (CYGNSS) mission. *IEEE Trans. Geosci. Remote Sens.*, **54**, 4419–4432, https://doi.org/10.1109/TGRS.2016.2541343.

Cui, Z., Z. Pu, V. Tallapragada, R. Atlas, and C. S. Ruf, 2019: A preliminary impact study of CYGNSS ocean surface wind speeds on numerical simulations of hurricanes. *Geophys. Res. Lett.*, **46**, 2984–2992, https://doi.org/10.1029/2019GL082236.

Dvorak, V. F., 1984: Tropical cyclone intensity analysis using satellite data. NOAA Tech. Rep. 11, 45 pp.

Gilleland, E., A. S. Hering, T. L. Fowler, and B. G. Brown, 2018: Testing the tests: What are the impacts of incorrect assumptions when applying confidence intervals or hypothesis tests to compare competing forecasts? *Mon. Wea. Rev.*, **146**, 1685–1703, https://doi.org/10.1175/MWR-D-17-0295.1.

Gleason, S., C. S. Ruf, M. P. Clarizia, and A. J. O'Brien, 2016: Calibration and unwrapping of the normalized scattering cross section for the cyclone Global Navigation Satellite System. *IEEE Trans. Geosci. Remote Sens.*, **54**, 2495–2509, https://doi.org/10.1109/TGRS.2015.2502245.

——, ——, A. J. O'Brien, and D. S. McKague, 2019: The CYGNSS level 1 calibration algorithm and error analysis based on on-orbit measurements. *IEEE J. Sel. Top. Appl. Earth Obs. Remote Sens.*, **12**, 37–49, https://doi.org/10.1109/JSTARS.2018.2832981.

Goldenberg, S. B., S. G. Gopalakrishnan, V. Tallapragada, T. Quirino, F. Marks, S. Trahan, X. Zhang, and R. Atlas, 2015: The 2012 triply nested, high-resolution operational version of the Hurricane Weather Research and Forecasting System (HWRF): Track and intensity forecast verifications. *Wea. Forecasting*, **30**, 710–729, https://doi.org/10.1175/WAF-D-14-00098.1.

Hamill, T. M., 1999: Hypothesis tests for evaluating numerical precipitation forecasts. *Wea. Forecasting*, **14**, 155–167, https://doi.org/10.1175/1520-0434(1999)014<0155:HTFENP>2.0.CO;2.

Hoffman, R. N., 1982: SASS wind ambiguity removal by direct minimization. *Mon. Wea. Rev.*, **110**, 434–445, https://doi.org/10.1175/1520-0493(1982)110<0434:SWARBD>2.0.CO;2.

——, 1984: SASS wind ambiguity removal by direct minimization. Part II: Use of smoothness and dynamical constraints. *Mon. Wea. Rev.*, **112**, 1829–1852, https://doi.org/10.1175/1520-0493(1984)112<1829:SWARBD>2.0.CO;2.

——, and R. Atlas, 2016: Future observing system simulation experiments. *Bull. Amer. Meteor. Soc.*, **97**, 1601–1616, https://doi.org/10.1175/BAMS-D-15-00200.1.

——, S. M. Leidner, J. M. Henderson, R. Atlas, J. V. Ardizzone, and S. C. Bloom, 2003: A two-dimensional variational analysis method for NSCAT ambiguity removal: Methodology, sensitivity, and tuning. *J. Atmos. Oceanic Technol.*, **20**, 585–605, https://doi.org/10.1175/1520-0426(2003)20<585:ATDVAM>2.0.CO;2.

Huang, C.-Y., Y. Kuo, S. Chen, and F. Vandenberghe, 2005: Improvements in typhoon forecasts with assimilated GPS occultation refractivity. *Wea. Forecasting*, **20**, 931–953, https://doi.org/10.1175/WAF874.1.

——, and Coauthors, 2010: Impact of GPS radio occultation data assimilation on regional weather predictions. *GPS Solut.*, **14**, 35–49, https://doi.org/10.1007/s10291-009-0144-1.

Kalnay, E., 2002: Atmospheric Modeling, Data Assimilation, and Predictability. Cambridge University Press, 341 pp.

Kuo, Y.-H., H. Liu, Y.-R. Guo, C.-T. Terng, and Y.-T. Lin, 2009: Impact of FORMOSAT-3/COSMIC data on typhoon and mei-yu prediction. *Recent Progress in Atmospheric Sciences: Applications to the Asia-Pacific Region*, K.-N. Liou and M.-D. Chou, Eds., World Scientific, 458–483.

Landsea, C. W., and J. L. Franklin, 2013: Atlantic hurricane database uncertainty and presentation of a new database format. *Mon. Wea. Rev.*, **141**, 3576–3592, https://doi.org/10.1175/MWR-D-12-00254.1.

Leidner, S. M., B. Annane, B. McNoldy, R. Hoffman, and R. Atlas, 2018: Variational analysis of simulated ocean surface winds from the Cyclone Global Navigation Satellite System (CYGNSS) and evaluation using a regional OSSE. *J. Atmos. Oceanic Technol.*, **35**, 1571–1584, https://doi.org/10.1175/JTECH-D-17-0136.1.

Leroux, M.-D., and Coauthors, 2018: Recent advances in research and forecasting of tropical cyclone track, intensity, and structure at landfall. *Trop. Cyclone Res. Rev.*, **7**, 85–105, https://doi.org/10.6057/2018TCRR02.02.

Liu, H., J. Anderson, and Y. Kuo, 2012: Improved analyses and forecasts of Hurricane Ernesto's genesis using radio occultation data in an ensemble filter assimilation system. *Mon. Wea. Rev.*, **140**, 151–166, https://doi.org/10.1175/MWR-D-11-00024.1.

McNoldy, B., B. Annane, S. J. Majumdar, J. Delgado, L. Bucci, and R. Atlas, 2017: Impact of assimilating CYGNSS data on tropical cyclone analyses and forecasts in a regional OSSE framework. *Mar. Technol. Soc. J.*, **51**, 7–15, https://doi.org/10.4031/MTSJ.51.1.1.

Mueller, M. J., A. C. Kren, L. Cucurull, S. P. F. Casey, R. N. Hoffman, R. Atlas, and T. R. Peevey, 2020: Impact of refractivity profiles from a proposed GNSS-RO constellation on tropical cyclone forecasts in a global modeling system. *Mon. Wea. Rev.*, **148**, 3037–3057, https://doi.org/10.1175/MWR-D-19-0360.1.

Phunthirawuthi, P., F. Wu, and P. Boonyuen, 2016: Performance analysis of GPS radio occultation assimilation for tropical cyclone monitoring. *2016 IEEE Int. Geoscience and Remote Sensing Symp. (IGARSS)*, Beijing, China, Institute of Electrical and Electronics Engineers, 2181–2184.

Ruf, C., and R. Balasubramaniam, 2019: Development of the CYGNSS geophysical model function for wind speed. *IEEE J. Sel. Top. Appl. Earth Obs. Remote Sens.*, **12**, 66–77, https://doi.org/10.1109/JSTARS.2018.2833075.

——, A. Lyons, M. Unwin, J. Dickinson, R. Rose, D. Rose, and M. Vincent, 2013: CYGNSS: Enabling the future of hurricane prediction. *IEEE Geosci. Remote Sens. Mag.*, **1**, 52–67, https://doi.org/10.1109/MGRS.2013.2260911.

——, S. Gleason, A. Ridley, R. Rose, and J. Scherrer, 2017: The NASA CYGNSS mission: Overview and status update. *2017 IEEE Int. Geoscience and Remote Sensing Symp. (IGARSS)*, Fort Worth, TX, Institute of Electrical and Electronics Engineers, 2641–2643.

——, ——, and D. S. McKague, 2019: Assessment of CYGNSS wind speed retrieval uncertainty. *IEEE J. Sel. Top. Appl. Earth Obs. Remote Sens.*, **12**, 87–97, https://doi.org/10.1109/JSTARS.2018.2825948.

Velden, C. S., and Coauthors, 2006: The Dvorak tropical cyclone intensity estimation technique: A satellite-based method that has endured for over 30 years. *Bull. Amer. Meteor. Soc.*, **87**, 1195–1210, https://doi.org/10.1175/BAMS-87-9-1195.

WHO, 2020: Tropical cyclones. WHO, accessed 9 September 2020, https://www.who.int/health-topics/tropical-cyclones#tab=tab_1.

WMO, 2020: 40th anniversary of the WMO Tropical Cyclone Programme. WMO, accessed 30 July 2020, https://public.wmo.int/en/our-mandate/focus-areas/natural-hazards-and-disaster-risk-reduction/tropical-cyclones.

Zhang, S., Z. Pu, D. J. Posselt, and R. Atlas, 2017: Impact of CYGNSS ocean surface wind speeds on numerical simulations of a hurricane in observing system simulation experiments. *J. Atmos. Oceanic Technol.*, **34**, 375–383, https://doi.org/10.1175/JTECH-D-16-0144.1.